Climate Dynamics (2021) 56:4091–4108
https://doi.org/10.1007/s00382-021-05688-x

Clustering circulation in eastern Asia as a tool for exploring possible mechanisms of extreme events and sources of model error

Robin T. Clark[1] · **Lixia Zhang**[2,3] · **Chaofan Li**[4]

Received: 15 September 2020 / Accepted: 30 January 2021 / Published online: 21 February 2021

Abstract
Every summer in eastern Asia, the combined effects of complex topography, multiple potential moisture sources and a mixture of sub-tropical and mid-latitude dynamics produces an environment, in which subtle differences in spatial patterns of atmospheric circulation can profoundly affect the geographic distribution of rainfall. Understanding and quantifying these patterns is a fundamental requirement if we are to understand, predict or project rainfall events likely to cause impacts to society in the region. To help the scientific community with this task, a method is presented here, in which spatial patterns of summer sea level pressure over eastern Asia are clustered into a set of eight circulation types, with examples given of their potential use. We find that the within-season prevalence of individual circulation types exhibit a strong relationship with the seasonal progression of the summer monsoon whilst providing a spatially coherent, physical interpretation of the monsoon for all parts of eastern Asia. Beyond this, the clustering approach permits the attribution of notable rainfall anomalies in almost any location within the domain used to build the clusters. Examples are given, showing how circulation specific moisture transport anomalies in one part of China can result in anomalously dry days in another part of the country. Two further applications of the clustering approach are demonstrated using climate simulations. The first is of circulation specific model errors which can allow targeted model development. The second provides information about anomalies which are plausible, but have yet to be observed, possibly due to limitations in the observed record.

Keywords Circulation · Clustering · Uncertainty · Climate · Rainfall variability · Asian monsoon

1 Introduction

Summer rainfall variability, on several scales, both temporally and spatially has profound economic and social impacts throughout eastern Asia in almost every year (e.g. Zong and Chen 2000; Shen et al. 2007; Huang et al. 2007; Hao et al. 2010; Qian et al. 2012; Yi et al. 2012). This is mostly driven by large scale spatial variability of circulation patterns in the region. Unfortunately, these patterns and their role on rainfall are highly complex. Depending on the circulation (see Supplementary Fig. 1 for the mean summer flow), moisture is potentially available for rainfall, from the Pacific Ocean, South China Sea, Bay of Bengal and even parts of Eurasia (Guo et al. 2018; Zhao et al. 2020). The Tibetan plateau and other mountain ranges in the region also exert a big influence on local circulation and act as a barrier to moisture. Furthermore, there is a mix, of sub-tropical and mid-latitude dynamics at play, depending on the latitude, and influences from circulation outside the region, most notably from the West Pacific Subtropical High (WPSH). To understand, and project future possible, climate change induced, impacts of rainfall, necessary for adaptation preparation therefore requires identification, understanding and quantification of the day-to-day variability of the dominant circulation patterns in the region.

✉ Robin T. Clark
robin.clark@metoffice.gov.uk

[1] Met Office Hadley Centre, Met Office, FitzRoy Road, Exeter EX1 3PB, UK

[2] LASG, Institute of Atmospheric Physics (IAP), Chinese Academy of Sciences (CAS), Beijing, China

[3] Collaborative Innovation Center on Forecast and Evaluation of Meteorological Disasters, Nanjing University of Information Science & Technology, Nanjing 210044, China

[4] Center for Monsoon System Research, Institute of Atmospheric Physics (IAP), Chinese Academy of Sciences, Beijing, China

A second purpose for the identification of circulation patterns stems from their potential use in forecasting, as proxies of rainfall. This should be possible since circulation is a driver prognostic and a key transporter of water vapour, thus exerting a strong control on precipitation. The ability of models to correctly simulate large-scale, observed circulation patterns is also likely to be greater than their ability to simulate rainfall (Zhang and Zhou 2015), which requires parametrisation of sub-grid scale processes, which themselves, are complex in the region, again for the reasons mentioned above.

A third reason for the pattern approach, is to convey information which is useful over a wide geographic area without losing information of local importance. In the absence of this approach, a forecast or a study of an event, focussing exclusively on an individual region is often of little benefit outside of that region. Using this approach also helps to avoid the need to define study regions beforehand, which can sometimes affect conclusions.

To identify the principal circulation patterns, Empirical Orthogonal Functions and Principal Component Analysis have sometimes been used (e.g. Yang et al. 2013, Ummenhofer et al. 2013) but these can be difficult to understand physically. Modified clustering approaches used in many fields of science provide other alternatives (e.g. Rodriguez and Laio 2014). One of these, "GrossWetterLagen" developed by Baur et al. (1944) and updated by Hess and Brezowsky (1952, 1969, 1977) subjectively classified European circulation based on local knowledge of weather impacts. An objective version of this was developed by James (2007) using spatial, daily fields of sea level pressure and geopotential height. Neal et al. (2016) adapted a k-means alternative, using sea level pressure only.

Neal et al's approach produces a set of specific spatial circulation patterns using an iterative algorithm in which daily spatial fields of sea level pressure (SLP) anomalies, with respect to a predefined period, are moved repeatedly between collections of fields in order to minimize the sum of within-cluster variance. For each collection, hereafter "cluster", a centroid pattern can be produced from the mean of the days in each cluster.

Throughout this paper, we use clusters defined over eastern Asia using a slightly modified version of Neal et al's approach applied to daily sea level pressure fields of 1979 to 2018 from the ERA5 reanalysis (Hersbach 2020). More details are given in Sect. 2. In this section, the issue of the number of clusters deemed most suitable, is also dealt with.

The aim of the rest of this paper is to provide a series of examples, demonstrating just some of the wide variety of analysis opportunities which circulation clustering can provide. In Sect. 3, this includes analysis of the WPSH, East Asian summer monsoon and fields such as rainfall, water vapour transport and temperature on the days of each of the SLP clusters. In Sect. 4, the already defined ERA5 SLP clusters are applied to simulations from two ensembles of climate models. A simple assessment is given, of each ensemble's ability to simulate the ERA5 frequency of the circulation types, followed by an examination of simulated rainfall anomalies in each type. To conclude Sect. 4, a novel use of the clustering approach is introduced, allowing an insight into the plausibility of rainfall anomalies exceeding those in the ERA5 record.

2 Method and data description

2.1 Clustering method and data

To address the issues mentioned in Sect. 1, we applied a slightly modified version of Neal et al's k-means based method to daily, spatial "latitude x longitude" fields of SLP anomalies from the ERA5 (Hersbach 2020) reanalysis dataset of 1979 to 2018. We used SLP here since, spatially, it is the largest primary driver of circulation (and its resulting local weather) over mid-latitude regions. Model performance at reproducing large scale observed SLP patterns is also likely to be better than of small-scale weather phenomena, affected by local topography. Unlike Neal et al., we use SLP from a rectangular box over eastern Asia (80° to 130° E, 18° to 50° N). Our focus throughout this paper is on the climatologically wet June, July and August (JJA) summer season in East Asia because of its impacts. For this reason, only SLP fields from JJA are used to define the clusters. All anomalies mentioned are relative to JJA climatology.

Throughout the paper, we use ERA5 as an estimate of real-world observations due to its temporal completeness and high horizontal (30km) resolution. For rainfall, gridded observations from CN05.1 (Wu and Gao 2013) were also used.

Model simulations to be shown come from three ensembles of fully coupled ocean-atmosphere climate models: HadCM3-ESPPE (Murphy et al. 2014), HadGEM3-PPE (Yamazaki et al. 2021) and CMIP5 (Taylor et al. 2012). Each of these use observed greenhouse gas concentrations from 1850 to 2006 and prescribed values following a RCP8.5 pathway thereafter. We confine our analysis to the years (1979 to 2018) matching those of ERA5. Table 1 gives a summary of the ensembles used.

2.2 Number of clusters and model performance

A key benefit of k-means clustering is its ability to produce any desired number of clusters. Choosing a suitable number, on the other hand is a challenge and depends on a balance between a desire to extract interesting signals and the robustness of those signals. This is best illustrated using some

Table 1 Simulations in each ensemble

	Member methodology	Atmospheric resolution
HadCM3-ESPPE (Murphy et al. 2014)	57 perturbed parameter versions of HadCM3	2.5° × 3.75°
HadGEM3-PPE (Yamazaki et al. 2021)	15 perturbed versions of HadGEM3-GC3.05	60 km
CMIP5 (Taylor et al. 2012)	8 models used based on their performance (McSweeney, 2018): CCSM4, CESM1-BGC, CMCC-CM, CNRM-CM5, EC-EARTH, GFDL-ESM2G, HadGEM2-ES, MPI-ESM-MR.	0.7° to 2.0° × 0.75° to 2° depending on model

examples. Supplementary Fig. 2 shows a typical result from collating daily JJA SLP into 2 clusters with ERA5 rainfall, expressed as anomalies of the climatological mean, for the two clusters. Cluster dependence of the rainfall on circulation is bland, yielding few clues about possible mechanisms governing unusual anomalies. Extreme events are indistinguishable. The internal variability within each of the 2 clusters, i.e., between their component fields is also likely to be too large to be useful. Supplementary Fig. 3, on the other hand, which shows the rainfall anomalies from using 20 clusters, has a striking range of diversity, both regionally and between differing clusters. In many of the clusters, regions of opposite but substantial anomalies are remarkably close to each other. Such a large number of clusters offers a great boost to understanding regional rainfall patterns and extremes. The extra detail, however, can be quite overwhelming. Robustness of results can also become an issue, since, with more clusters, there are fewer days contributing to each cluster. In Supplementary Fig. 3, all clusters consist of at least 98 days.

To determine, objectively, a suitable minimum number of clusters for use in cluster analysis, the "elbow method" (Thorndike 1953) has often been used in the literature. For cluster sets of differing numbers of clusters, averages of the distances between cluster centroids and their component days are calculated, from which a curve is plotted, against the number of clusters. Typically, the resulting curve has a kink (or elbow), where the gradient of distances per number of clusters, clearly decreases, determining a suitable minimum number of clusters to use.

Using Euclidean distance and spatial correlation (between SLP fields) as measures of these distances, for the region of our focus though, gives curves (see Supplementary Fig. 4), whose gradients appear to decrease smoothly with cluster size, with any kinks difficult to identify. Points along the curve, however, which are further away from the diagonal between the top left and bottom right corners, suggest that a minimum of 6 clusters is desirable.

Beyond the elbow-curve statistics of observed clusters themselves, the ability of models in reproducing the observed properties of clusters is a further factor to consider if model simulations are to be used to foretell future climate variability. To examine this aspect, Supplementary Fig. 5 gives an assessment, for each of the HadCM3-ESPPE, HadGEM3-PPE and CMIP5 ensembles, of their ability to reproduce the ERA5 cluster frequencies, according to how many clusters are defined. For each predefined number of clusters, the ability was calculated for each member separately, for each relevant cluster. Two measures were used to quantify this: The mean (across relevant clusters) of the model simulated cluster frequency divided by the corresponding ERA5 frequency and correlations between the ERA5 cluster frequencies and those of each ensemble. These are shown in Supplementary Fig. 5a and b respectively. Values of 1.0 are desirable in both. From the top panel, with increasing cluster size, all three ensembles appear to overestimate the average cluster frequency. The ratio is closest to 1.0 using 7 or 8 clusters. Using correlation, the ability appears to decrease with cluster size.

Taking the above issues into account suggests that analysis based on 8 clusters is a reasonable approach for this *particular* region and season. From here-on in, all plots and discussion will be shown using 8 clusters. Analysis using 6 up to 12 clusters was, however completed for all the exercises. The results from using these differing numbers of clusters were very similar to those using 8 clusters.

3 Results from using 8 clusters based on ERA5

3.1 Circulation and relationship with the West Pacific Subtropical High

To verify that the SLP based clusters really do represent the actual circulation, Figs. 1 and 2 show anomalies (relative to the JJA climates shown in Supplementary Figs. 6a and b), for each cluster type, of the zonal and meridional ERA5 wind, 10m above the surface, averaged over the days in each circulation cluster. We show these two components separately here, rather than using combined vectors, since they are showing anomalies rather than actual winds. For some clusters (e.g. 1 and 6), the spatial anomaly patterns in the two wind components are also quite different. A further

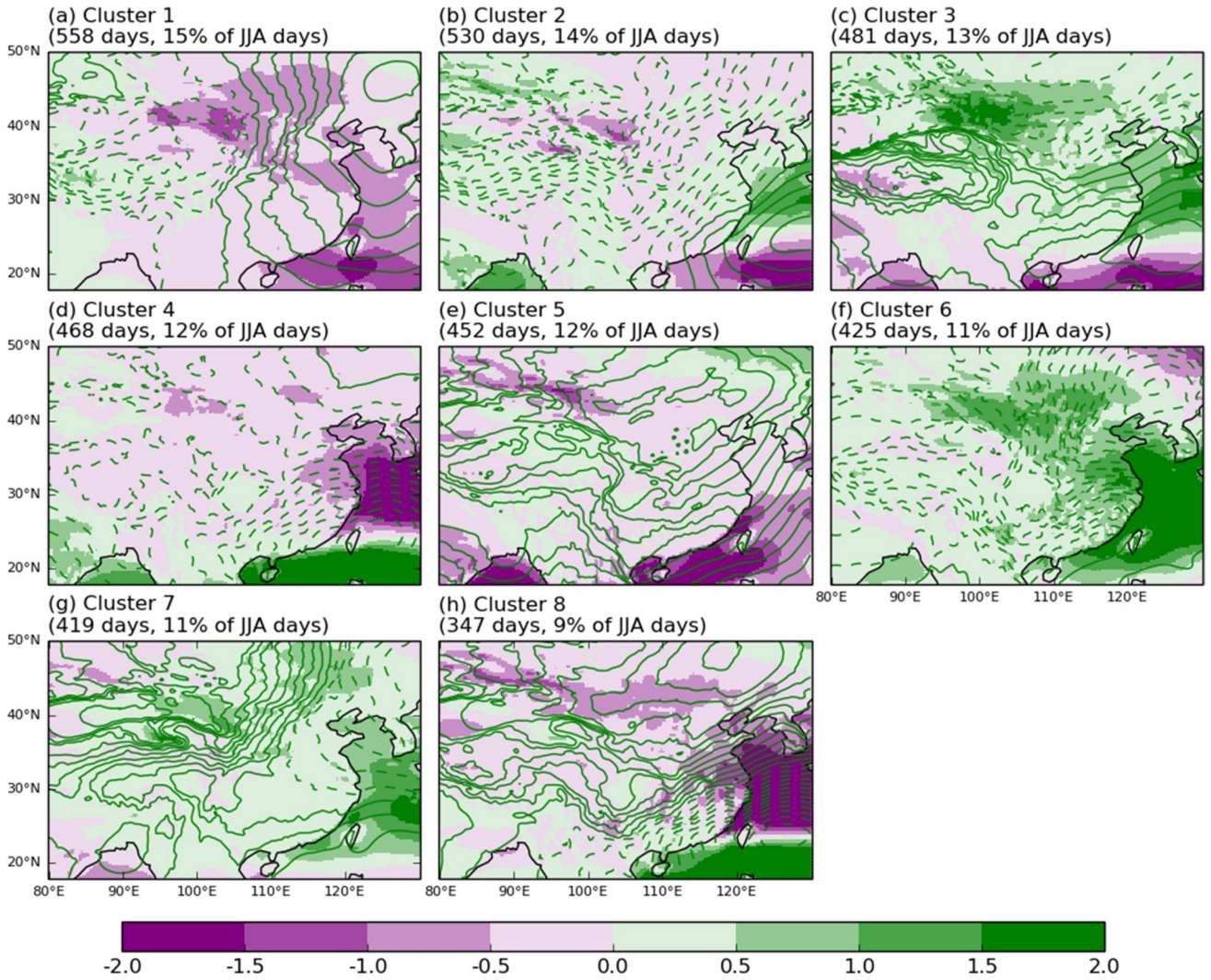

Fig. 1 Mean ERA5 10m zonal wind (ms^{-1}, green and purple shading) anomaly (with respect to JJA climate) of JJA 1979 to 2018 days in each ERA5 sea level pressure defined cluster. Dashed and solid contour lines show negative and positive anomalies respectively of the mean ERA5 sea level surface pressure anomaly (0.4 hPa intervals) in each cluster. Numbers in the panel titles indicate the number of days in each cluster

key benefit of not combining them will also emerge in the following Sect. 3.2 and later when considering their relationships with other meteorological fields - for example northward moisture flux. Maps of the windspeed anomalies expressed as vectors, however, are available in the Supplementary material (Supplementary Fig. 7). Considering some examples from Fig. 1, the positive zonal anomalies (green areas) in Clusters 2 and 3 over eastern China and the west Pacific are clearly the result of the positive anti-cyclonic SLP anomaly east of Taiwan shown by the centroid contours, around which, a clockwise flow anomaly would be expected. On the southern side of the pressure anomaly, a negative zonal flow anomaly (purple areas) is seen. Compared to clusters 2 and 3, a broadly opposite pattern is seen in, both clusters 4 and 8, related to the negative pressure anomaly close to Taiwan. This anomaly also manifests itself in a northerly anomaly on its left flank in these clusters in Fig. 2. In Fig. 2, Clusters 1 and 6 appear to be approximate opposites of each other with meridional flow anomalies of opposite signs, over northern China.

The quasi-stationary West Pacific subtropical (WPSH) anticyclone is an important component of circulation above the surface, particularly at 500 hPa, east of China during JJA (Rodwell and Hoskins 2001). To examine how the WPSH is related to our SLP clusters, Supplementary Fig. 8 shows the geopotential height of 500 hPa in each cluster and contours of the overall climatological mean. Values greater than 5885dam clearly show the position of the WPSH. Regarding the clusters discussed above; in clusters 2 and 3, the WPSH is stronger than normal and displaced towards Asia,

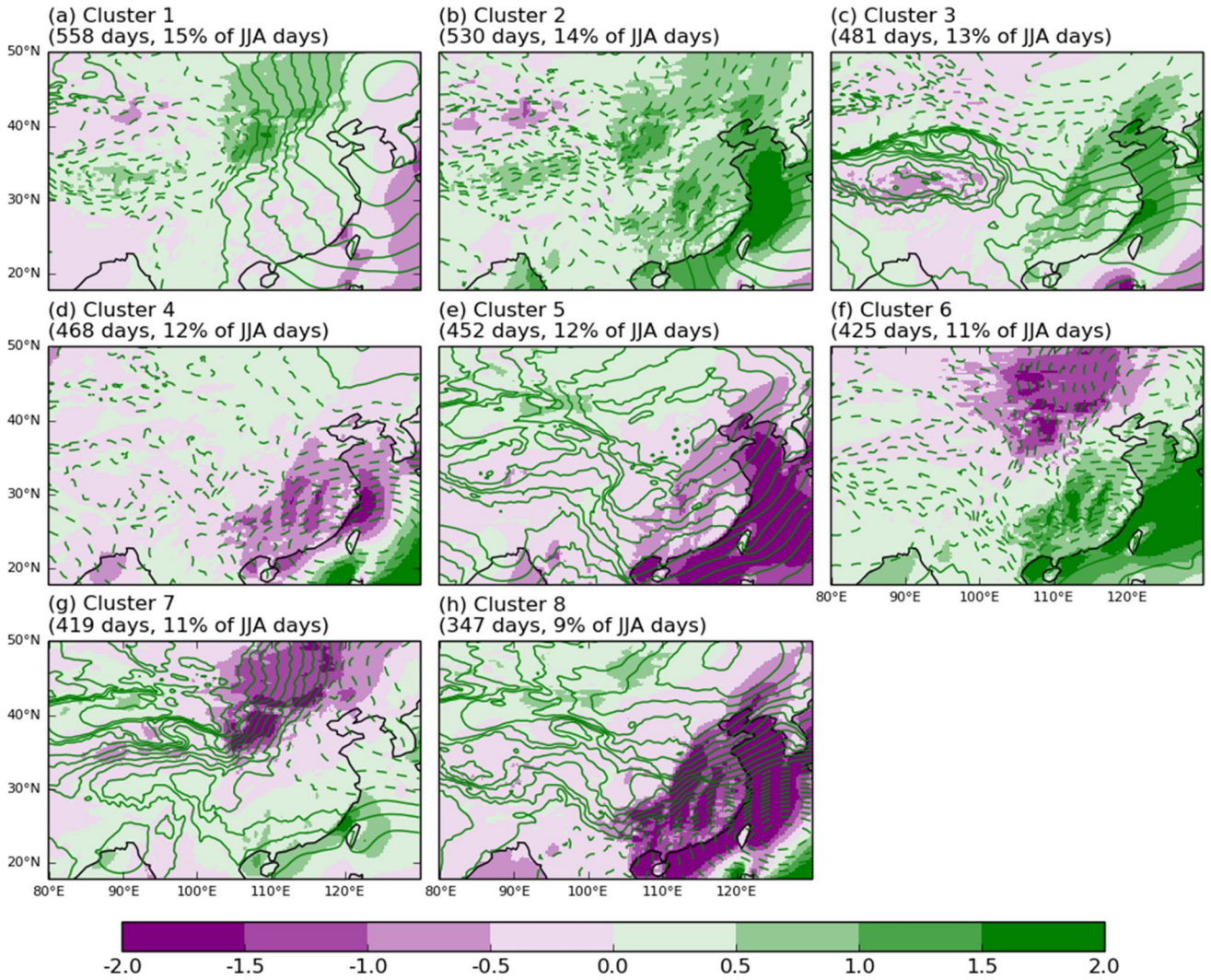

Fig. 2 Mean ERA5 10m meridional wind (ms^{-1}, green and purple shading) anomaly (with respect to JJA climate) of JJA 1979 to 2018 days in each ERA5 sea level pressure defined cluster. Dashed and solid contour lines show negative and positive anomalies respectively of the mean ERA5 sea level surface pressure anomaly (0.4 hPa intervals) in each cluster. Numbers in the panel titles indicate the number of days in each cluster

supporting the positive pressure anomalies at the surface. A very different pattern is seen in Clusters 4 and 8. In both, the WPSH is weaker than normal and eastward displaced. Interestingly, although the WPSH behaviour of Cluster 4 is very similar to that of Cluster 8, there are considerable differences in the sign of the surface pressure anomaly between the two, over mainland China. Surface pressure anomalies are negative in Cluster 4 but positive in Cluster 8, especially in the north away from the cyclonic anomaly over the West Pacific. The weaker influence of the WPSH on the surface pressure and circulation anomaly pattern in north China is also apparent in Clusters 1 and 6. The anticyclonic and cyclonic anomalies in this part of China are particularly pronounced, despite the WPSH in these two clusters being quite similar. Finally, the WPSH in Cluster 6 appears to be very similar to that of Cluster 7. Over eastern China however, the meridional flow in much weaker in Cluster 7.

3.2 Seasonal progression of cluster frequencies and relationship with monsoon

Large scale circulation over eastern Asia is characterised by a climatological northward transition from northerly flow during winter to southerly flow in summer. To determine how this transition is interpreted by the SLP clusters, Fig. 3a shows rolling 30-day means,averaged over all 1979 to 2018 years, of the frequencies of each cluster through the summer JJA months. Clusters 2 and 6, for example, become more frequent from early June to early July, and then less frequent, as summer proceeds, whilst clusters 5 and 8, which

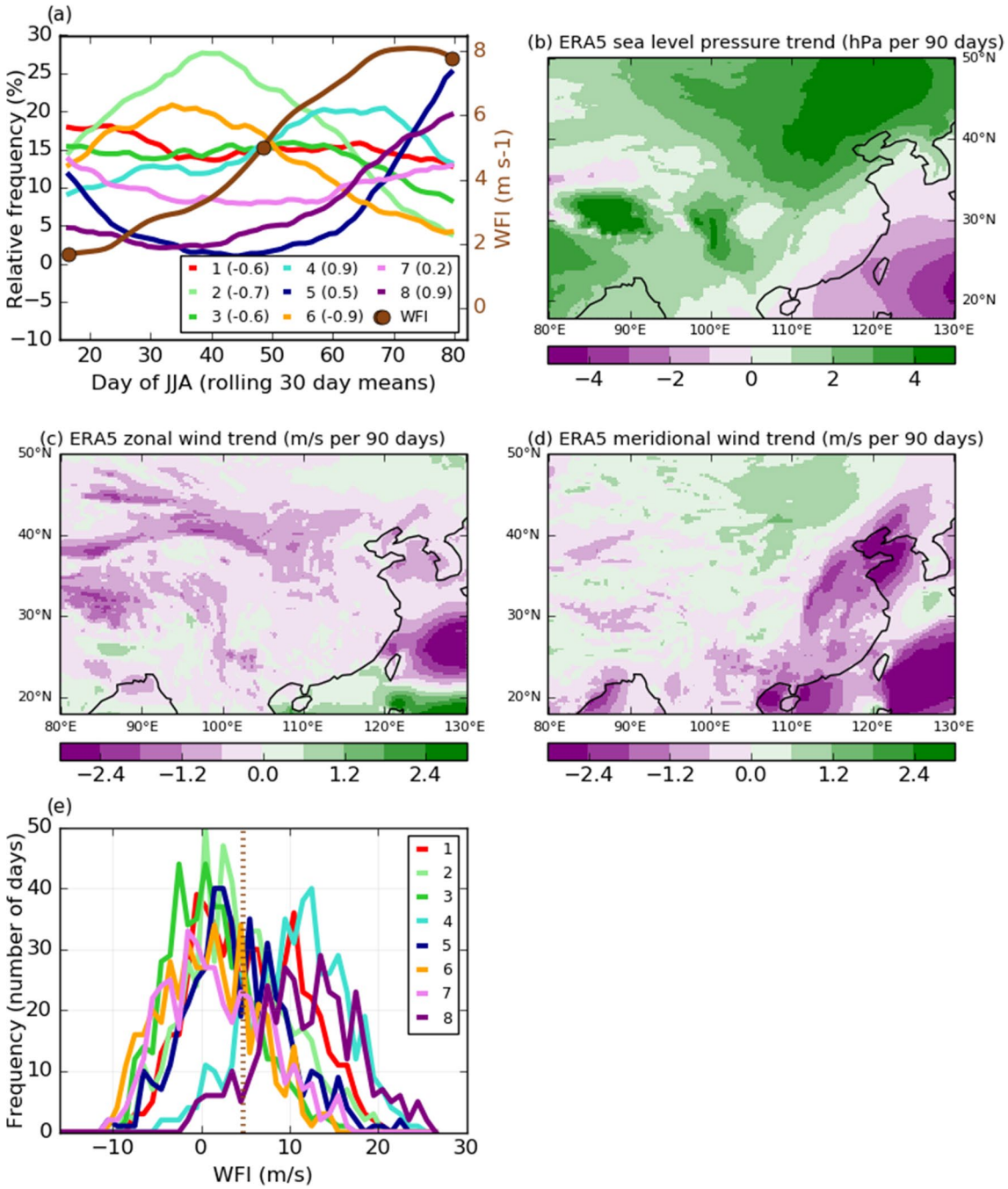

Fig. 3 **a** Relative frequency of each ERA5 sea level pressure defined cluster, of JJA days, averaged over the years 1979 to 2018 (all colours except brown, left axis) and corresponding, *regardless of cluster* East Asian summer monsoon Wang Fan Index (WFI, Wang and Fan 1999) values (brown line, right axis). The legend gives the cluster number and temporal correlation between each cluster's frequency and the WFI. **b–d** Linear (from fitting a polynomial) *within-season* trends of all 1979 to 2018 JJA days (irrespective of cluster), calculated separately in each year and then averaged over all years. **e** Distributions of WFI of JJA days in each cluster (coloured lines) and overall mean (vertical brown dotted line, 4.8 ms^{-1}) of all days, regardless of cluster

are associated with greater than normal SLP over the Asian continent, become more frequent. The changes in these can be clearly related to *within-season* trends (averaged over the whole ERA5 period) of sea-level pressure, zonal and meridional wind in each summer, shown in Fig. 3b–d. In Fig. 3b, for example, pressure builds over north-eastern China and decreases over the Pacific, so that towards the end of each summer, on average, cluster 8, characterised by positive and negative anomalies of pressure in these two regions, becomes more frequent. The opposing trends of zonal wind

(in Fig. 3c), around this negative pressure anomaly, are also clear and are very similar to those of Fig. 1h. The negative trend in the meridional wind seen over eastern China (Fig. 3d) is also as a manifestation of the weakening pressure over the Pacific Ocean. This is also seen in Fig. 2h.

Returning to Fig. 3a, the brown line allows a comparison to be made between the cluster frequencies and a widely used measure of the East Asian summer monsoon. For this, we use the Wang-Fan (Wang and Fan 1999) index (area averaged U_{850} over (5°–15°N, 90°–130°E) minus that over (22.5°–32.5°N, 110°–140°E), hereafter WFI. Clusters 4, 6 and 8 are most closely correlated, temporally (see legend of Fig. 3a), to the trend of the WFI due to their centres of action in the region of the index's definition. Other clusters have a weaker relationship, indicating their use in capturing variability beyond that of the monsoon.

Finally, Fig. 3e gives information showing how distributions of the frequency of each cluster sit within the overall range of WFI values, irrespective of the within-season trend. Clusters 4 and 8, typically occur when the WFI is greater than its overall mean (4.8m s^{-1}) unlike the other clusters. Days when the WFI is greater than normal, however, can and do occur in all cluster types. Even 20 % of the days of the two clusters (Clusters 3 and 6) whose WFI values are the most negative, occur when the index is greater than the mean.

3.3 Rainfall within SLP clusters

Figure 4 gives maps of the ERA5 rainfall, averaged over the days in each of the 8 clusters, expressed as a fraction of the overall JJA mean. Spatial correlations (given in panel titles) between the anomalies shown and equivalent values obtained using CN05.1 observations (see Supplementary Fig. 9 for plot using CN05.1) indicate broad agreement between the two datasets with similar large scale patterns of anomalies in both.

Large regions of rainfall deficit are seen in northern China in Clusters 2, 3 and 6. In Cluster 3, these appear to be associated with the anomalous anti-cyclonic anomaly over the Tibetan plateau and westerly flow anomalies (see Fig. 1c) from central Asia. In Cluster 6, the deficit is situated within a region of reduced meridional flow (from the south) compared to normal, seen in Fig. 2f. By examining anomalies of additional fields during this cluster, Fig. 5 provides an example of how the circulation clustering approach can help to objectively attribute the rainfall deficit. A reduced northward water vapour (WV) flux compared to normal (in red, Fig. 5a) dominates northern China in the cluster, almost certainly related to the negative meridional wind anomaly in the region. The absolute WV flux (not shown) even becomes southward in the region. The specific humidity (Fig. 5b) in the north is therefore much less than normal, as well as the total column water vapour (Fig. 5c) and cloud cover fraction (Fig. 5d). The reduced cloud cover itself appears to play a subsequent role on the 850 hPa temperature in the region which is warmer than normal (Fig. 5e). This is despite a southward wind anomaly, emanating from a region, further north, where the temperature anomaly is negative in this cluster. Within the warm anomaly, increased moisture is therefore required for the atmosphere to reach saturation, reflected in the reduced relative humidity in the region, shown in Fig. 5f.

Returning to Fig. 4; days are wetter than normal in the monsoon region of eastern China (east of 105°E) in Clusters 1 and 2. It is easy to see how anomalies in the position and magnitude of the surface pressure anomaly can explain this behaviour. In Supplementary Fig. 10a, the meridional flow is stronger than usual, transporting more moisture northwards than normal. In Supplementary Fig. 10b, the rainfall is visibly diverted towards the northeast, instead of the northwest, which consequently has a rainfall deficit.

Elsewhere, deficits are seen over the lower half of the Yangtze in Clusters 4 and 8. In these two clusters, the 500 hPa level WPSH (see Supplementary Fig. 8d and h) is weaker than normal and displaced to the east. As a consequence, the zonal flow (see Fig. 2d, h) and associated northward flux of water vapour (see Supplementary Figs. 10d and g) from the south, into the Yangtze region is less than normal. Anomalies of the fields of Fig. 5 for all other clusters are also shown in Supplementary Fig. 10.

To visualise how the circulation clusters contribute to specific parts of the daily rainfall distribution, Fig. 6a, b provide maps of the identity of the most frequent clusters during lower and upper quartile days of ERA5 rainfall, hereafter denoted as the driest and wettest days, respectively. The dependence on location, of the cluster identities contributing to the driest days is striking, and powerfully illustrates the challenges faced when attempting to attribute rainfall deficits in China. Three different circulation patterns, for example, are responsible over eastern China, depending on the location. The anomalies seen in the panels of Fig. 4 however, can be easily matched to the spatial patterns shown here. The deficits of Cluster 6, discussed earlier, for example, clearly result in this cluster being the most frequent, shown in pink, in Fig. 6a, during the driest days over northern China. Spatial coherence between differing regions is also notable. Cluster 6, for example, is the most frequent during the driest days, not only in north China, but also in southern China and Vietnam.

Equivalent maps using the CN05.1 rainfall observations are shown in Supplementary Fig. 11. Although there are some similarities, the most frequent clusters are identical to those from ERA5, in only 0.45 % and 0.6 % of the CN05.1 area. The differences between the ERA5 and CN05.1 results arise from disagreements between two data sources

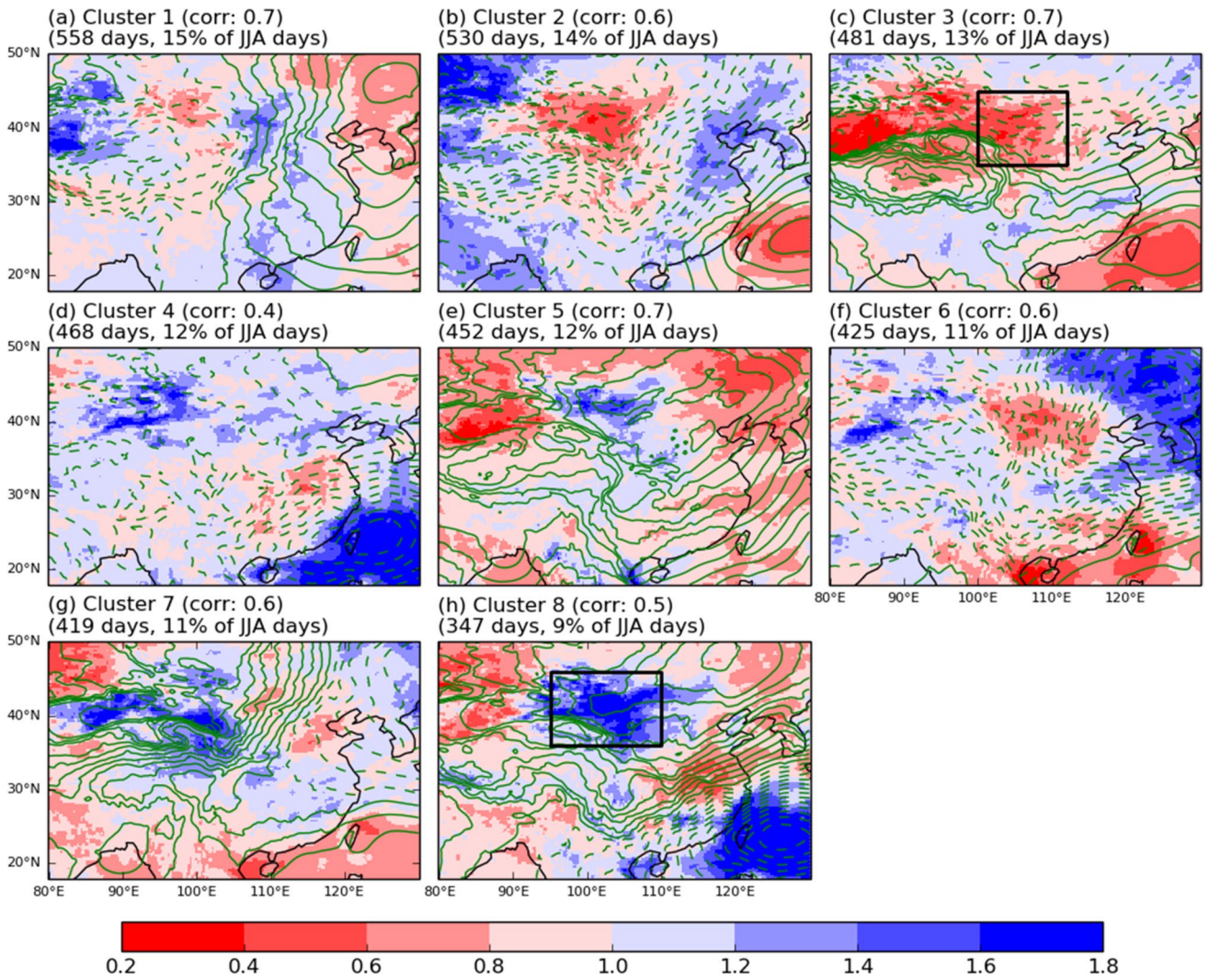

Fig. 4 ERA5 rainfall averaged over JJA 1979 to 2018 daysin each cluster, as a fraction of overall (regardless of cluster) JJA climate. Avalue of 2.0, for example, shows rainfall twice the climate. Dashed and solid contourlines show negative and positive anomalies respectively of the mean ERA5 sealevel surface pressure anomaly (0.4 hPa intervals) in each cluster. "Corr:" value in panel titles is spatialcorrelation with equivalent rainfall fractions obtained using observed CN05.1rainfall (see Supplementary Fig. 6). The black boxes are discussed in Sect. 3.4

regarding the days contributing to the lower and upper quartiles. From Supplementary Fig. 12, for example, it appears that over most parts of China, no more than 50 % of the days deemed by ERA5 to be in the lower quartile of rainfall are also in the corresponding lower quartile of CN05.1. The discrepancy is likely to be related to small differences between the gamma-like nature of ERA5 and CN05.1 daily rainfall distributions.

Returning to Fig. 6; panels c, d show the relative area of the land surface where each cluster is the most frequent during the driest and wettest days. Considering the driest and wettest days together, suggests that Cluster 1 is likely to be associated with the widest areal extent of impacts from rainfall anomalies. This is also true, according to the CN05.1 observations (see Supplementary Fig. 11 panels c and d). Maps (not shown) of cluster frequencies contributing to the most extreme 10 % and 5 % of, both, the driest and wettest days give similar large-scale patterns, but with considerably more noise. In 0.68 and 0.53 of the overall domain (in terms of area), the clusters were the same in the driest 10 % and 5 % of days. For the wettest 10 % and 5 % of days, the fractions were 0.69 and 0.57 respectively.

3.4 Distribution of daily rainfall in each cluster

In addition to the findings of Fig. 6 discussed above, there are also, for the two regions shown by the black boxes in Fig. 6a, b, some further, rather unexpected results

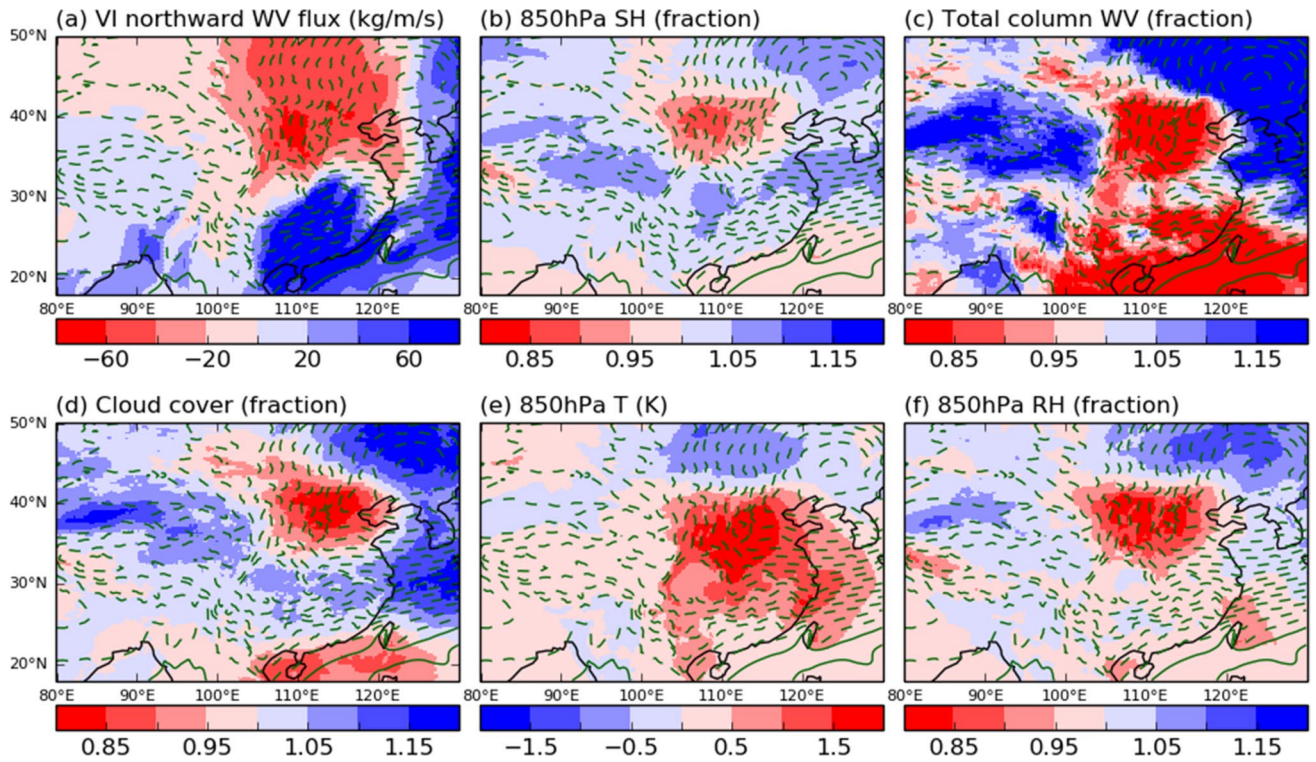

Fig. 5 Mean ERA5 values of six diagnostics during JJA1979 to 2018 days of Cluster 6. **a**, **e** are shown as anomalies compared tooverall JJA climate. **b**–**d**, **f** are shown as fractions of theclimate. *VI* Vertically integrated, *WV* Water vapour, *SH* specific humidity, *T* temperature, *RH* relative humidity. Dashed and solidcontour lines show negative and positive anomalies respectively of the meanERA5 sea level surface pressure anomaly (0.4 hPa intervals) in the cluster

requiring further examination. Cluster 3 contributes very little to the box in Fig. 6a, despite an actual rainfall deficit (see black box area in Fig. 4c) greater than in other clusters. Likewise, Cluster 8 is absent from the box in Fig. 6b, despite this cluster giving (see Fig. 4h), on average, large positive anomalies. Indeed, Cluster 8 is even almost entirely absent from all panels of Fig. 6. To examine this result, Fig. 7a, b gives the distribution of daily rainfall intensity from the days in each cluster for the two black boxes respectively. For each intensity category, the relative frequency contributions from each cluster to the overall frequency, is remarkably consistent, regardless of rainfall intensity. Clusters 1 and 8 are the most and least frequent, for example, reflecting the values shown in the panel titles of Fig. 4. In Fig. 7a, Clusters 1 and 2 are more frequent than Cluster 3 for all rainfall intensities contributing to the lower quartile (whose intensity is shown by the vertical dotted line) of overall daily rainfall. In Fig. 7b, Cluster 8 is the least frequent cluster for all intensities in the upper quartile (to the right of the dotted line) up to days when the rainfall intensity fraction (of the overall climate) is 2.5. The effect suggests that caution is advised if cluster probabilities are to be used to infer the likelihood of extreme events.

4 Model ability in simulating the circulation clusters

4.1 Ability to reproduce observed cluster frequency

Good reproduction in climate models, of observed circulation characteristics is a necessary condition if projections of climate change using these models are to be beneficial for impact mitigation and management. Figures 4 and 6 have shown how this includes the intensity and frequency of circulation regimes. Figure 8 therefore shows the frequency of each cluster during 1979 to 2018 JJA days of the ERA5 and HadCM3-ESPPE, HadGEM3-PPE and CMIP5 ensembles. For most clusters, the full ensemble ranges reasonably encompass the ERA5 frequencies (green bars), but the interquartile ranges generally do not. The decline of ERA5 cluster frequencies as the cluster number increases is captured well by all three ensembles with correlations between the ensemble means and ERA5 of at least 0.75. The HadCM3-ESPPE performs most poorly. For this reason, this ensemble is excluded from analysis here-on.

To explore possible reasons for the differences between the simulated and ERA5 frequencies, Fig. 9 shows how the sea level pressure patterns on each day of each cluster

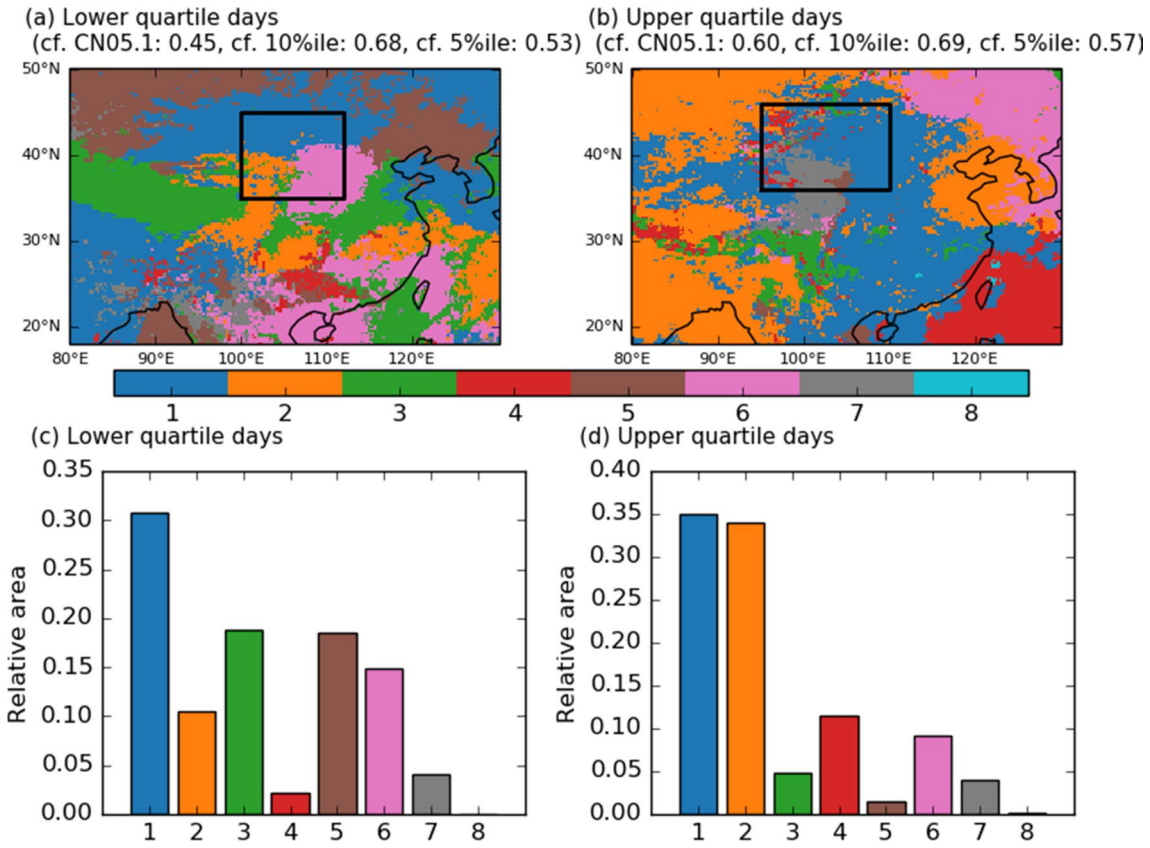

Fig. 6 Top row: Identity of most frequent clusterduring days of **a** less than and **b** greater than lower and upper quartile thresholdsrespectively, of JJA 1979 to 2018 ERA5 rainfall (Quartile thresholds calculated separately at eachgridbox). The1st number in the title of each panel shows the fraction of theCN05.1 area (which has less coverage) where CN05.1 gives the same results asERA5. The 2nd and 3rd numbers are the fractions of thearea in which the clusters of the most extreme 10% and 5% of days, are the sameas those of the quartile days). The black boxes are the same as in Fig. 4c,i, and are discussed in Sect. 3.4. Bottom row: Total relativespatial area where each cluster is the most frequent in the domainscorresponding to **a** and **b** respectively

compare to the centroid pressure patterns (the contours shown, for example, in Fig. 1) of the cluster which they are deemed to be in. The comparisons are shown as distributions of Euclidean distance from the centroid for both ERA5 (in green) and the HadGEM3-PPE simulations (in purple). As expected, the distributions are centred close to 0. They are wide, however, such that in all clusters, in both the ERA5 reanalysis and PPE simulations, there are many days of greater distances from the centroid of their cluster. The existence of these days, a consequence of the attempt to pigeon-hole the natural variability of sea level pressure, into just eight types, results in many days contributing to the frequency diagnostics of Fig. 8, even though they may only be weakly associated with the cluster which they are deemed to belong to. This situation appears particularly stark in clusters 1 and 3 (Fig. 9a, c). The mean of the correlations (see panel titles of Fig. 9) between the ERA5 and PPE distributions was also the weakest in these two clusters. Results, however, from a simple comparison (not shown), between these correlations (from all clusters) and the model frequency errors shown in Fig. 8 gave no evidence of a link.

Despite the shortcomings in the cluster frequency performances of the HadGEM3-PPE and CMIP5 ensembles, potentially reducing the credibility of probabilistic projections for the region, model simulations of the weather (e.g. rainfall) within clusters can still be useful by adopting a conditional "During days of Cluster X, you are likely to have an average of Y" approach.

4.2 Ability of models to reproduce observed cluster dependent rainfall

Figure 10 shows the equivalent of Fig. 4, but from the HadGEM3-PPE simulations. For each HadGEM3-PPE simulation, the mean fraction of that simulation's climate mean (regardless of circulation cluster) rainfall was calculated for the days of each simulation deemed to be in each cluster. The ensemble mean (HadGEM3-PPE EM) of these fractions is shown in Fig. 10. The large scale, spatial patterns

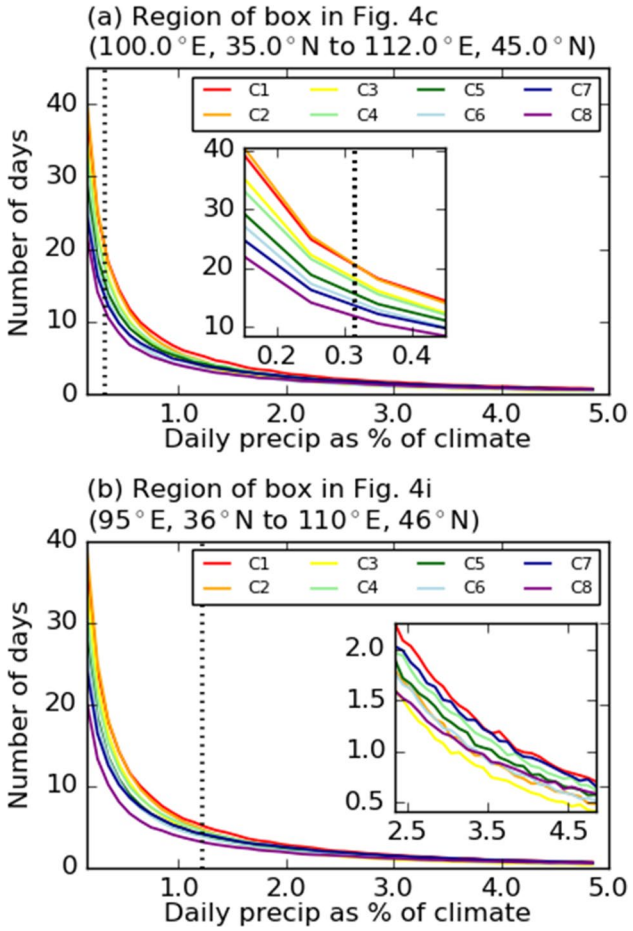

Fig. 7 Distribution of daily JJA precipitation areaaveraged for the boxes shown in Fig. 4c, i, in each SLP cluster (denoted Cin legend). Inset image is an expansion of two parts of the spectrum. Verticaldotted line in the top and bottom panel shows the 25th and 75th percentile of daily rainfall respectively

of the fractions are very similar in both figures. Spatial correlations between the two (shown in the title of each plotted panel of Fig. 10) exceeding 0.8 in all clusters, showing a strong fidelity of HadGEM3-PPE simulated rainfall to the sea level pressure patterns. CMIP5 ensemble mean rainfall (Supplementary Fig. 14) gives very similar results.

For a more direct comparison with the ERA5 anomalies, Fig. 11 shows the HadGEM3-PPE EM rainfall as a fraction of the corresponding, cluster dependent ERA5 rainfall for each cluster, giving indications of how circulation dependent model rainfall biases contribute to overall mean biases, typically shown in the literature. Regions of red and blue show where the HadGEM3-PPE EM is either too dry or too wet. Certain characteristics of the biases appear to occur in all clusters. The EM is too dry, for example, between 35°N and 59°N, west of 90°E, and too wet to the east, regardless of cluster. The magnitude, spatial extent and location of areas of other bias aspects, however, appear to be somewhat cluster dependent suggesting that overall mean bias quantities can potentially be misleading. Over Eastern China, between Shanghai and Beijing (between 30°N and 40°N), for example, a dry bias is seen in most clusters, but not in Clusters 4 and 8, suggesting that during days of a negative zonal wind anomaly, characteristic in both of these clusters, it would be wrong to correct the HadGEM3-PPE rainfall by applying a mean bias. Similar types of conclusions also arise from CMIP5 equivalent rainfall biases (shown in Supplementary Fig. 14).

Possible reasons for the differing biases can be gleaned by comparing other HadGEM3-PPE diagnostics of similar types to those of ERA5, shown in Fig. 5, for the same cluster. Figure 12 shows an example using Cluster 6. Given that the clusters of days in the HadGEM3-PPE simulations are identified solely using sea level pressure patterns, and that each cluster (including Cluster 6) contains days of a relatively wide range of these patterns (discussed in Sect. 4.1, using Fig. 9), the plots of Fig. 12 are remarkably like those

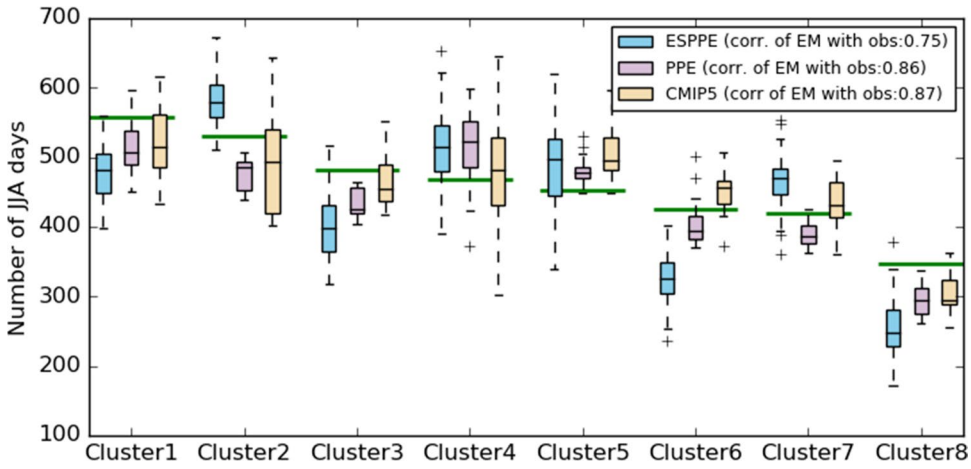

Fig. 8 Cluster dependent frequencies of JJA 1979 to2018 days in each cluster. Boxes show inter-quartile ranges across ensemblemembers. Whiskers show full range. Horizontal green lines show ERA5 frequencies

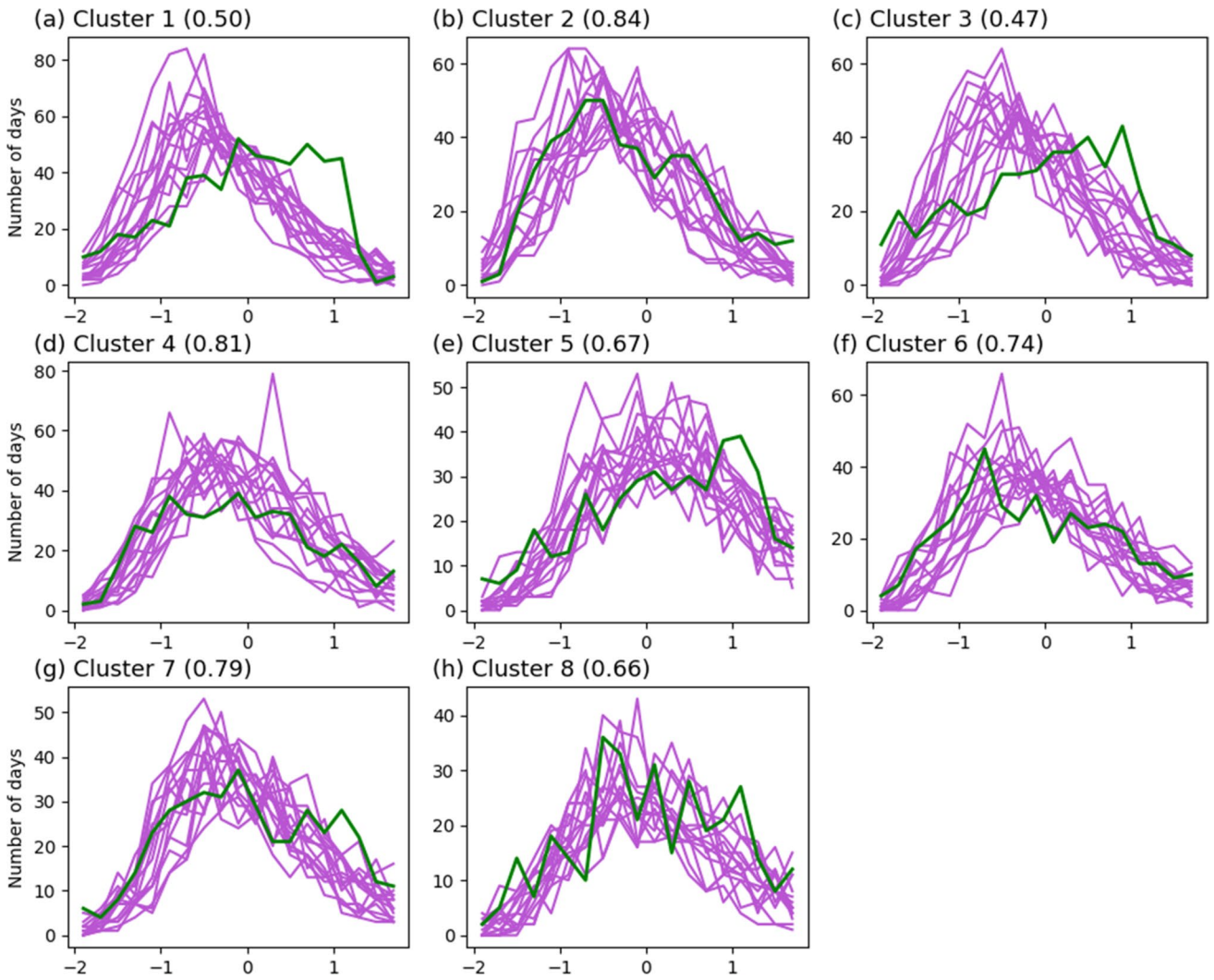

Fig. 9 Distributions of daily Euclidean distance (xaxis) normalised by its standard deviation between normalised sea levelpressure (SLP) of JJA 1979 to 2018 days in each cluster, and the centroid ofeach cluster. Y-axis shows the number of days for each normalised distance bin(bins of 0.2 width). Green and violet lines show the results from the ERA5 andHadGEM3-PPE simulations respectively. The number in the panel titles is the meanof the correlations between the green and violet lines. Normalisation wascarried out by dividing the relevant distances from each day, by thecorresponding ERA5 and PPE standard deviations of the distances, *regardless*of cluster

of Fig. 5. Supplementary Fig. 15 gives the biases of the diagnostics of Fig. 12, compared to ERA5. Some of these are clearly related to the rainfall biases of Fig. 11 f. Over eastern China, for instance, the simulated cloud cover and 850 hPa relative humidity is less than in ERA5, corresponding to the negative rainfall bias in the region in cluster 6.

4.3 Use of the ensembles to quantify unseen events

Figure 4, discussed earlier, showed the cluster dependence of ERA5 rainfall anomalies for the period 1979 to 2018. The period, however, is unlikely to have been long enough to have captured the full range of plausible anomalies associated with each cluster which could have theoretically occurred since 1979 but did not, due to chance. Examples of observed events absent from ERA5, because they occurred before 1979, include, for example, some of the severest droughts of the past century in North America and eastern China during the 1960s (Shen 2007).

Furthermore, analysis of influences on rainfall, from remote teleconnections, requires observations from several decades, at least, to achieve reliable results, due to subtle spatial and intensity differences in, and between, short and long term ocean circulation cycles such as the Pacific Decadal and Atlantic Multidecadal oscillations (e.g. Sterl et al. 2007; Wang et al. 2014).

To gain an estimate of what could have happened, if, for example, many more decades of ERA5 were available, we

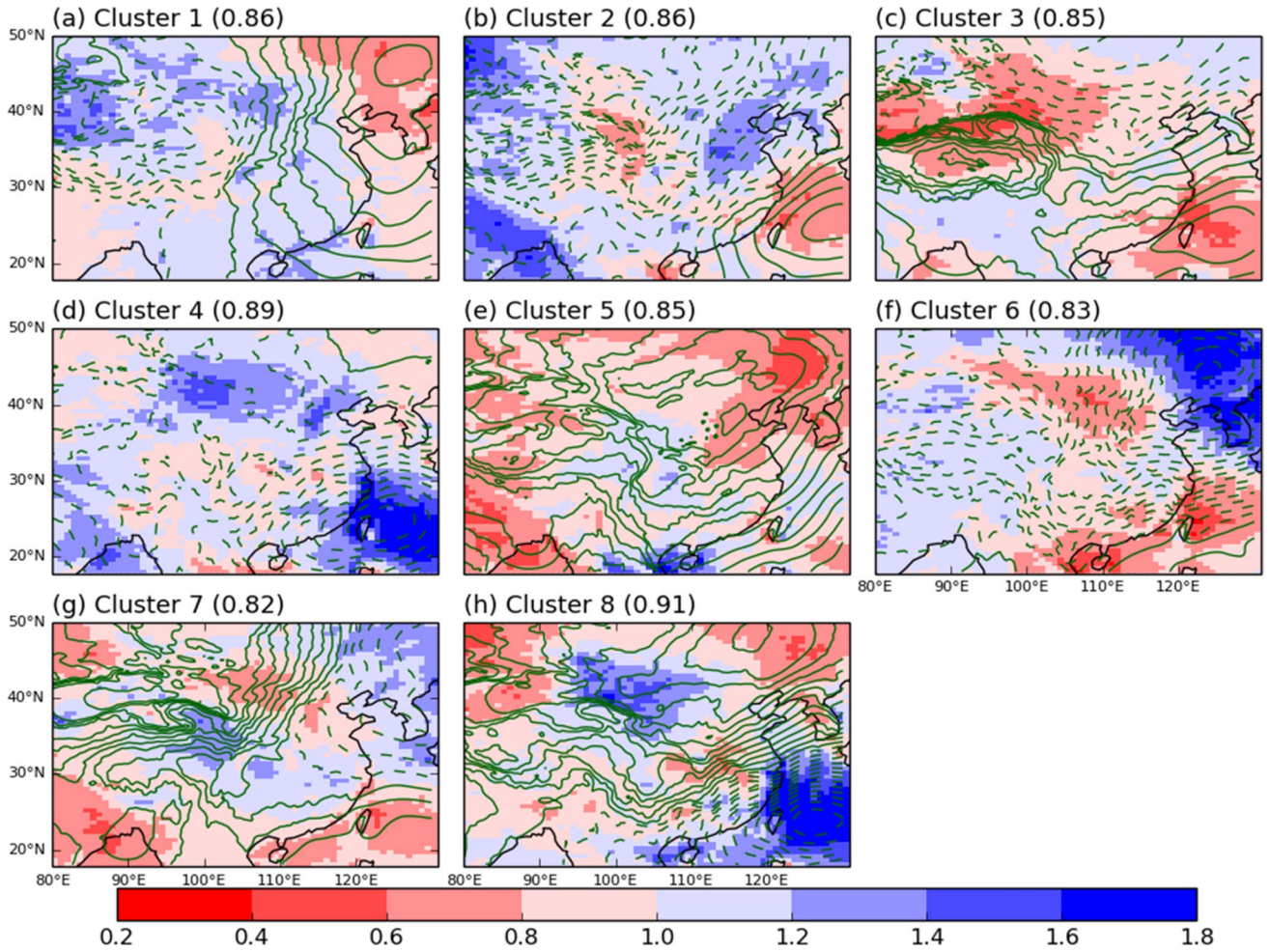

Fig. 10 Mean HadGEM3-PPE rainfall (blue and red shading) as a fraction of JJA HadGEM3-PPE climate (climate calculated separately for each HadGEM3-PPE simulation) during JJA 1979 to 2018 days in each ERA5 sea level pressure defined cluster. Thenumber in the panel titles is the spatial correlation between the values plotted and those of the corresponding ERA5 rainfall fraction shown in Fig. 4. Dashed and solid contour lines show negative and positive anomalies respectively of the mean ERA5 sea level surface pressure anomaly (0.4 hPa intervals) in eachcluster

can harness the diversity of the individual members of the HadGEM3-PPE and CMIP5 ensembles. Since, we are interested in the rainfall in individual clusters, expressed as a fraction of the overall mean, we can, subject to caveats, treat individual simulations of the ensembles as additional quasi-realisations of the 1979 to 2018 period, using an approach similar to that used by Thompson et al. (2017).

To do this, the individual HadGEM3-PPE rainfall simulations, expressed as fractions of the climate of each simulation (from which the ensemble mean was calculated, separately for each cluster, for Fig. 10) were ranked at each model gridbox. Figures 13 and 14 show the 10th and 90th percentiles of the ranked fractions respectively, divided by the corresponding ERA5 fractions (shown in Fig. 4). Enhanced deficits are seen for several locations in Clusters 3, 5 and 8 and the region of deficits discussed earlier in Cluster 6. Enhanced surpluses to note (in Fig. 14), are those on the northern flank of the cyclonic SLP anomalies of Clusters 4 and 8, east of China. Similar results are shown for equivalent CMIP5 percentiles in Supplementary Figs. 16 and 17.

There are caveats to bear in mind, however, with this exercise. One is the fact that the HadGEM3-PPE and CMIP5 ensembles have too few simulations to give a true range of all plausible outcomes, both in terms of the rainfall and circulation. The aim here is to simply highlight this role of clustering in providing extra information about events likely to have large impacts. Spatial coherence of the anomaly enhancements is also not guaranteed, i.e. enhancements at differing gridboxes may come from differing simulations.

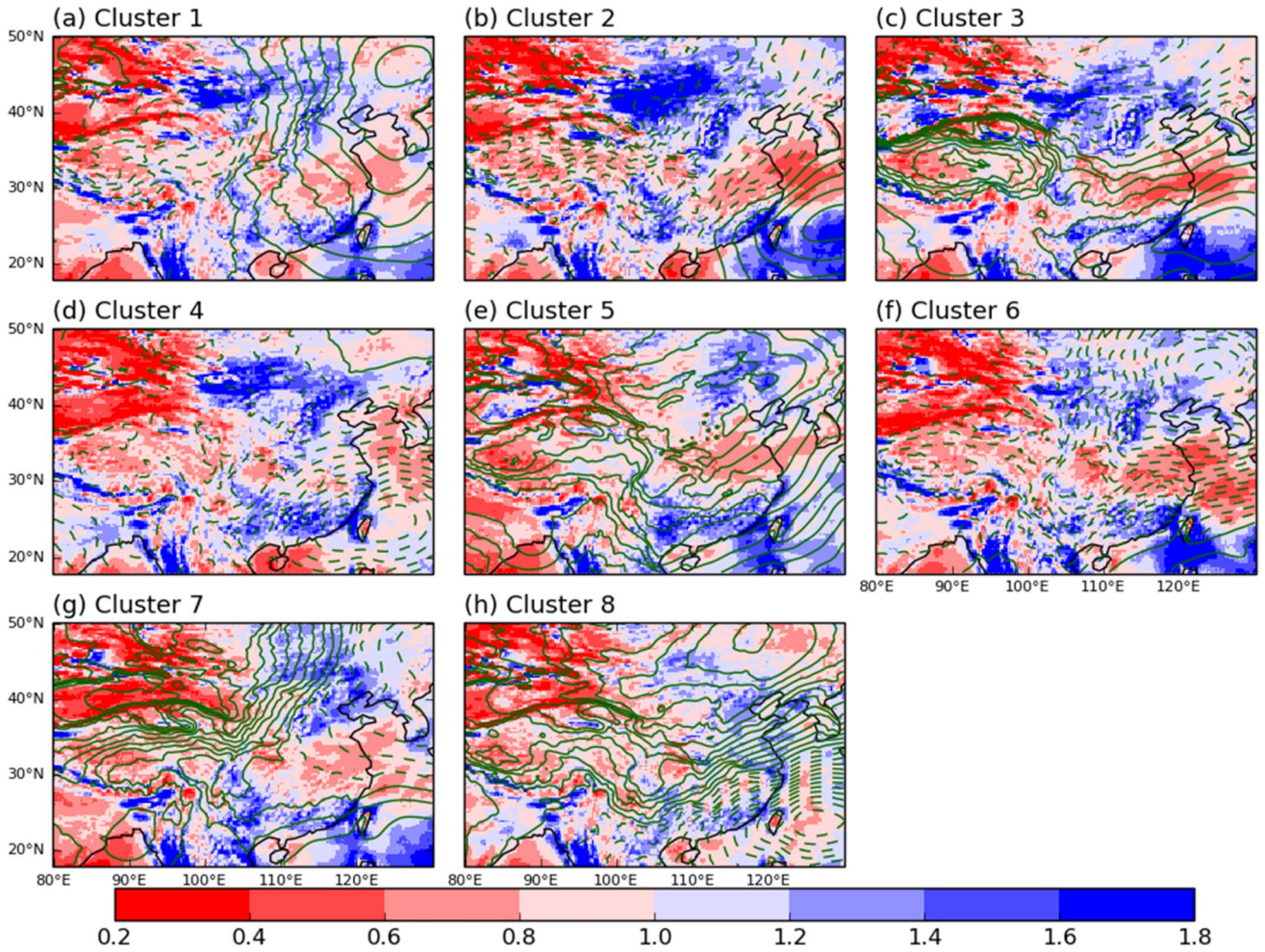

Fig. 11 Mean HadGEM3-PPE rainfall (blue and red shading)as a fraction of the corresponding cluster's ERA5 mean rainfall during JJA 1979to 2018 days in each ERA5 sea level pressure defined cluster. A value of 2.0shows where the HadGEM3-PPE is twice as wet as the ERA5 value in that cluster. Dashedand solid contour lines show negative and positive anomalies respectively of themean ERA5 sea level surface pressure anomaly (0.4 hPa intervals) in eachcluster

5 Conclusions

The overall aim of this paper has been to demonstrate how an easy-to-use, objective method, of circulation clustering can be used to capture and consolidate the complex nature of daily circulation variability in East Asia into a form useful for further research.

A set of 8 circulation cluster patterns relevant to east Asia were produced by applying a clustering algorithm to ERA5 re-analyses of sea level pressure from JJA days in 1979 to 2018. The individual patterns exhibited a variety of distinct surface level manifestations of anomalies of the mid-level (500 hPa) climatological West Pacific Subtropical High (WPSH). In some of these, the WPSH was displaced and in others, was weaker or stronger than normal. Evolution of the East Asian summer monsoon was found to be related to within season changes in the frequency of most, but not all the cluster patterns showing that the clusters give information beyond that explained by the monsoon alone.

Spatial patterns of ERA5 re-analysis anomalies of wind velocity, rainfall, moisture transport and temperature were found to be highly cluster pattern dependent and within each pattern, were strongly spatially correlated. Using an example, the clustering approach was found to be a useful tool for the attribution of spatial rainfall anomaly patterns. The circulation dependent spatial patterns of rainfall, seen

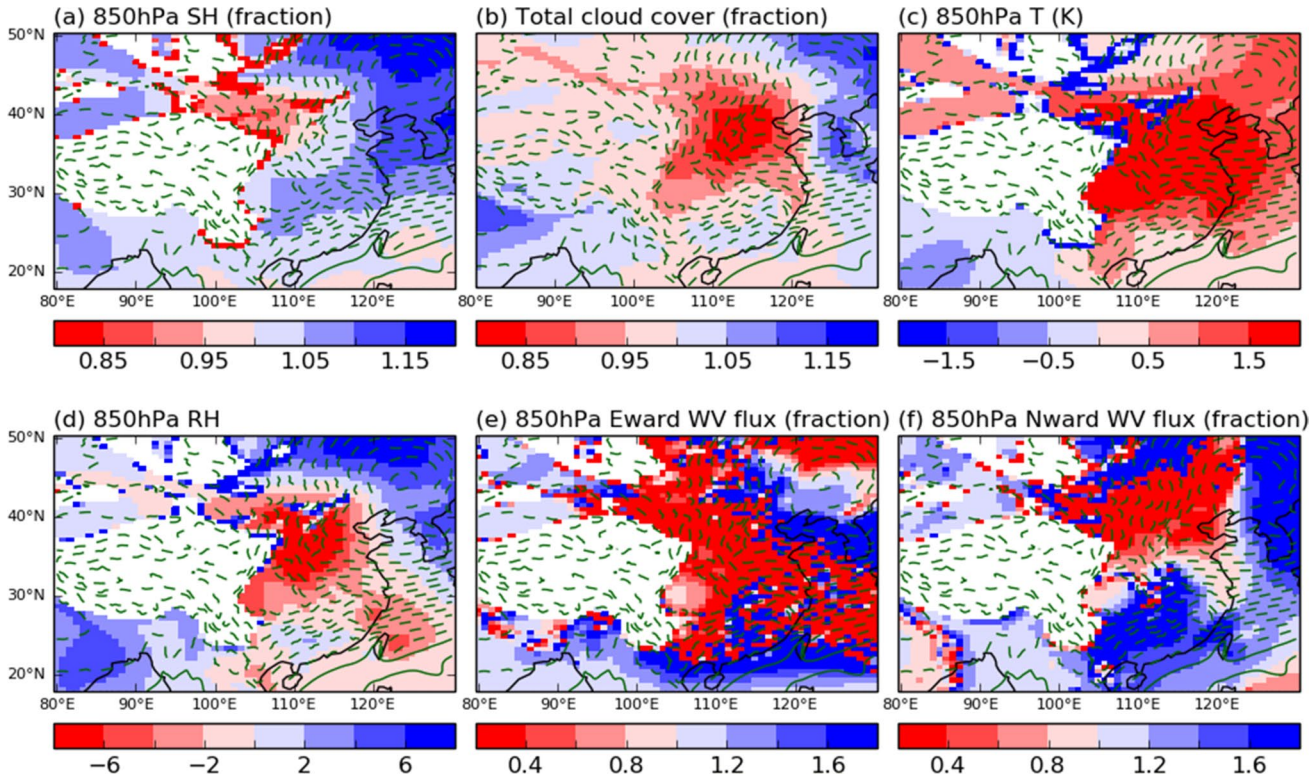

Fig. 12 Mean HadGEM3-PPE values of six diagnostics, during JJA 1979 to 2018 days in ERA5 sea level pressure defined Cluster 6, for comparison with those of Fig. 5. **a**, **b**, **e**, **f** Are shown as fractions of their relevant'regardless of cluster' JJA climates. **c**, **d** Are shown as anomalies fromtheir relevant 'regardless of cluster' JJA climates. Dashed and solid contourlines show negative and positive anomalies respectively of the mean ERA5 sealevel surface pressure anomaly (0.4 hPa intervals) in each cluster

in the ERA5 reanalyses were replicated remarkably well by climate models from two ensembles. This suggests a possible role for circulation clusters as proxy predictions of rainfall for locations where models predict circulation well but perform poorly at rainfall. In such locations, the clustering approach also yielded information about potential causes of the model rainfall bias, useful for model development. While some bias patterns occurred regardless of circulation cluster, others were cluster specific.

In a final demonstration of the use of circulation clustering, evidence was found that anomalies of rainfall greater than the most extreme of those found in ERA5 were plausible during the 1979 to 2018 period, potentially providing a method of examining extreme events not in the observed record.

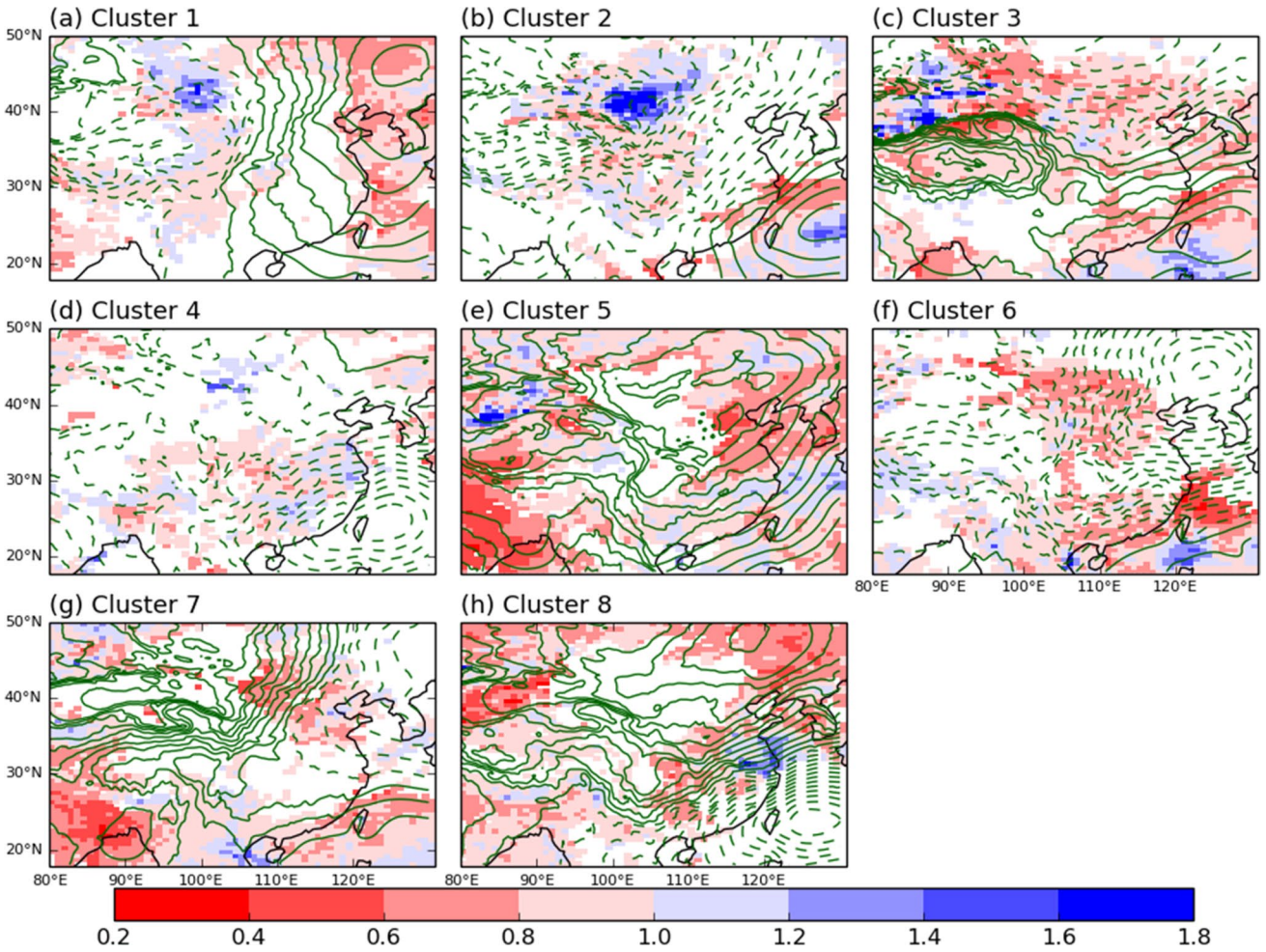

Fig. 13 Cluster dependent 10th percentile of ranked HadGEM3-PPE-fractions of corresponding HadGEM3-PPE simulation climate (during JJA 1979 to 2018 days) divided by the equivalent ERA5 fraction in each cluster. Mask applied tolocations where ERA5 rainfall in a cluster is greater than the overall climate. A value of 0.5, for example, shows a HadGEM3-PPE fraction which is half the equivalent ERA5 fraction. Dashed and solid contour lines show negative and positive anomalies respectively of the mean ERA5 sea level surface pressure-anomaly (0.4 hPa intervals) in each cluster

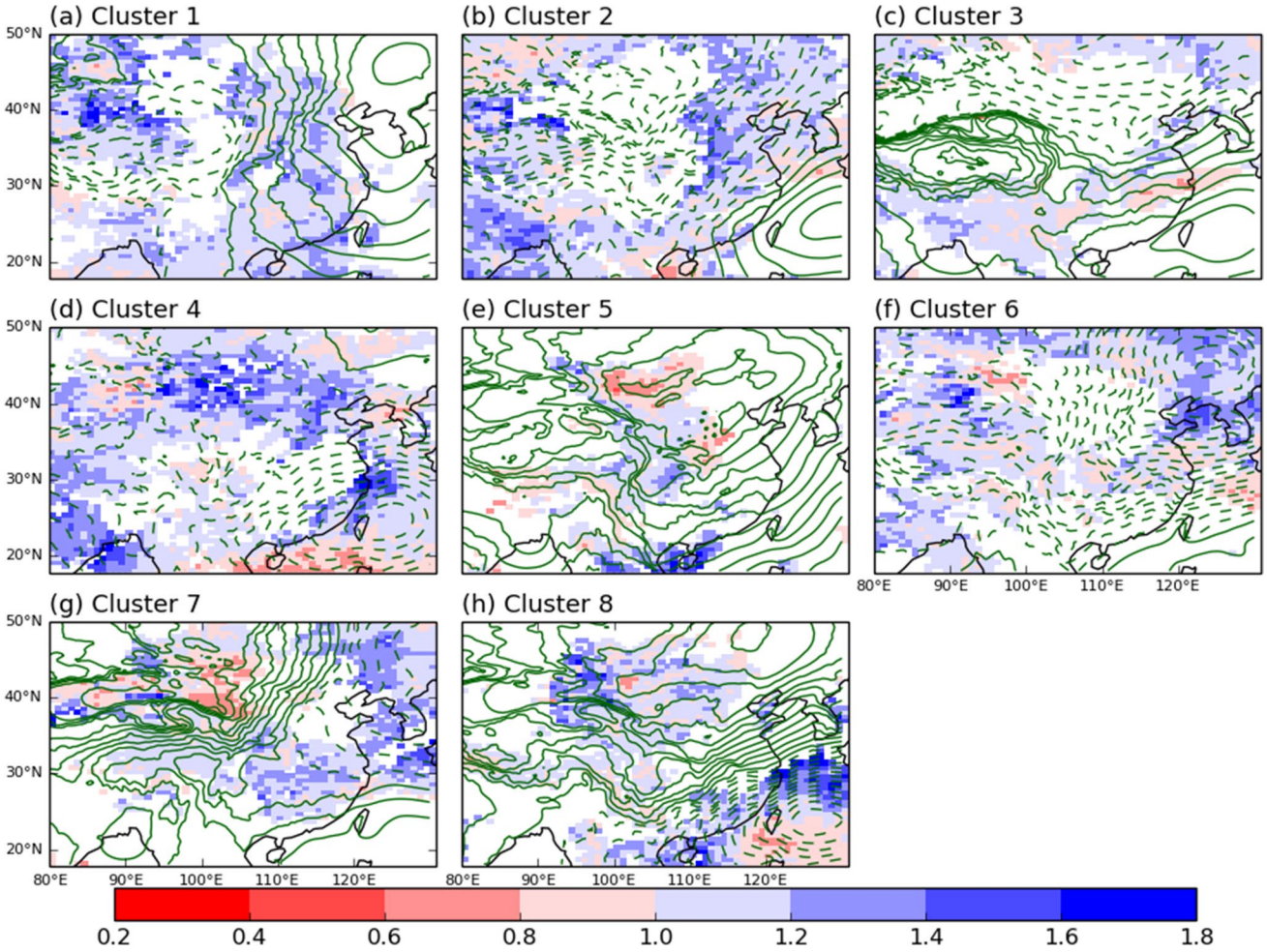

Fig. 14 As Fig. 13, but of the 90th percentile of ranked HadGEM3-PPE simulations. A value of 2.0, for example, shows where a HadGEM3-PPE simulated fraction is twice as large as the corresponding ERA5 fraction. Mask applied to locations where ERA5 rainfall in a cluster is less than the overall climate. Dashed and solid contour lines show negative and positive anomalies respectively of the mean ERA5 sea level surface pressure anomaly (0.4 hPa intervals) in each cluster

Supplementary Information The online version contains supplementary material available at https://doi.org/10.1007/s00382-021-05688-x.

Acknowledgements Robin Clark was supported by the UK-China Research & Innovation Partnership Fund through the Met Office Climate Science for Service Partnership (CSSP) China as part of the Newton Fund. Lixia Zhang was supported by the National Natural Science Foundation of China under Grant Nos. 42075037, 41675076 and the Innovative Team Project of Lanzhou Institute of Arid Meteorology (GHSCXTD-2020-2). Chaofan Li was supported by the National Key Research and Development Program of China (2018YFC1506005).

Compliance with ethical standards

Conflict of Interest The authors declare thatthey have no conflict of interest.

References

Baur F, Hess P, Nagel H (1944) Kalender der Grosswetterlagen Europas 1881–1939. Bad Homburg Rep

Enomoto T, Hoskins BJ, Matsuda Y (2003) The formation mechanism of the Bonin high in August. Quart J Roy Meteor Soc 129:157–178. https://doi.org/10.1256/qj.01.211

Gao H, Yang S (2009) A severe drought event in northern China in winter 2008–2009 and the possible influences of La Niña and Tibetan Plateau. J Geophys Res Atmos. https://doi.org/10.1029/2009JD012430

Guo L, Klingaman NP, Demory ME et al (2018) The contributions of local and remote atmospheric moisture fluxes to East Asian precipitation and its variability. Climate Dyn 51:4139–4156. https://doi.org/10.1007/s00382-017-4064-4

Hao Z, Zheng J, Wu G, Zhang X, Ge Q (2010) 1876–1878 severe drought in North China: facts, impacts and climatic background. Chin Sci Bull 55(26):3001–3007. https://doi.org/10.1007/s11434-010-3243-z

Hersbach H, Bell B, Berrisford P, Hirahara S, Horányi A, Muñoz-Sabater J, Nicolas J, Peubey C, Radu R, Schepers D, Simmons A (2020) The ERA5 global reanalysis. Q J Royal Met Soc Jul 146(730):1999–2049. https://doi.org/10.1002/qj.3803

Hess P, Brezowsky H (1952) Katalog der GrosswetterlagenEuropas 1881–1976. Berichte des Deutschen Wetterdienstes in der US-Zone, 33

Hess P and Brezowsky H (1969) Katalog der Grosswetterlagen Europas 1881–1976. 2nd ed. Berichte des Deutschen Wetterdienstes 113

Hess P and Brezowsky H (1977) Katalog der Grosswetterlagen Europas 1881–1976. 3rd ed. Berichte des Deutschen Wetterdienstes 113

Huang R, Sun F (1992) Impacts of the tropical western Pacific on the East Asian summer monsoon. J Meteor Soc Japan 70:243–256

Huang R, Chen J, Huang G (2007) Characteristics and variations of the East Asian monsoon system and its impacts on climate disasters in China. Adv Atmos Sci 24(6):993–1023. https://doi.org/10.1007/s00376-007-0993-x

James PM (2007) An objective classification method for Hess and Brezowsky Grosswetterlagen over Europe. Theor Appl Cli-matol 88:17–42. https://doi.org/10.1007/s00704-006-0239-3

Jia Wu, Xue-Jie G (2013) A gridded daily observation dataset over China region and comparison with the other datasets (in Chinese). Chin J Geophys Chin Ed 56:1102–1111. https://doi.org/10.6038/cjg20130406

Lamb HH (1972) British Isles Weather Types and a Register of the Daily Sequence of Circulation Patterns 1861–1971. Geo-physical Memoirs, Vol. 116, HMSO:85

Li C, Scaife AA, Lu R, Arribas A, Brookshaw A, Comer RE, Li J, MacLachlan C, Wu P (2016) Skillful seasonal prediction of Yangtze river valley summer rainfall. Environ Res Lett. https://doi.org/10.1088/1748-9326/11/9/094002

Murphy JM, Booth BB, Boulton CA, Clark RT, Harris GR, Lowe JA, Sexton DM (2014) Transient climate changes in a perturbed parameter ensemble of emissions-driven earth system model simulations. Climate dynamics 43(9–10):2855–2885. https://doi.org/10.1007/s00382-014-2097-5

Neal R, Fereday D, Crocker R, Comer RE (2016) A flexible approach to defining weather patterns and their application in weather forecasting over Europe. Meteorol Appl 23(3):389–400. https://doi.org/10.1002/met.1563

Qian W, Shan X, Chen D, Zhu C, Zhu Y (2012) Droughts near the northern fringe of the East Asian summer monsoon in China during 1470–2003. Clim Change 110(1–2):373–383. https://doi.org/10.1007/s10584-011-0096-7

Rodriguez A, Laio A (2014) Clustering by fast search and find of density peaks. Science 344(6191):1492–1496. https://doi.org/10.1126/science.1242072

Rodwell MJ, Hoskins BJ (2001) Subtropical anticyclones and summer monsoons. J Clim 14(15):3192–3211

Shen C, Wang WC, Hao Z, Gong W (2007) Exceptional drought events over eastern China during the last five centuries. Clim Change 85(3–4):453–471. https://doi.org/10.1007/s10584-007-9283-y

Sterl A, van Oldenborgh GJ, Hazeleger W, Burgers G (2007) On the robustness of ENSO teleconnections. Clim Dyn 29(5):469–85. https://doi.org/10.1007/s00382-007-0251-z

Taylor KE, Stouffer RJ, Meehl GA (2012) An overview of CMIP5 and the experiment design. Bull Am Meteor Soc 93(4):485–498. https://doi.org/10.1175/BAMS-D-11-00094.1

Thompson V, Dunstone NJ, Scaife AA, Smith DM, Slingo JM, Brown S, Belcher SE (2017) High risk of unprecedented UK rainfall in the current climate. Nat Commun. https://doi.org/10.1038/s41467-017-00275-3

Thorndike RL (1953) Who belongs in the family? Pyschometrika 18(4):267–276. https://doi.org/10.1007/BF02289263

Ummenhofer CC, D'Arrigo RD, Anchukaitis KJ, Buckley BM, Cook ER (2013) Links between Indo-Pacific climate variability and drought in the Monsoon Asia Drought Atlas. Clim Dyn 40(5–6):1319–1334. https://doi.org/10.1007/s00382-012-1458-1

Wang B, Fan Z (1999) Choice of South Asian summer monsoon indices. Bull Am Meteorol Soc 80(4):629–38. https://doi.org/10.1175/1520-0477(1999)080<0629:COSASM>2.0.CO;2

Wang S, Huang J, He Y, Guan Y (2014) Combined effects of the Pacific decadal oscillation and El Nino-southern oscillation on global land dry–wet changes. Sci Rep 4:6651. https://doi.org/10.1038/srep06651

Yamazaki K, Sexton DMH, Rostron JW, McSweeney CF, Harris GR, Murphy JM (2021) A perturbed parameter ensemble of HadGEM3-GC3.05 coupled model projections: Part 2: global performance and future changes. Clim Dyn (accepted)

Yang F, Shi F, Kang S, Wang S, Xiao Z, Nakatsuka T, Shi J (2013) Comparison of the dryness/wetness index in China with the Monsoon Asia Drought Atlas. Theor Appl Climatol 114(3–4):553–566. https://doi.org/10.1007/s00704-013-0858-4

Yi L, Yu H, Ge J, Lai Z, Xu X, Qin L, Peng S (2012) Reconstructions of annual summer precipitation and temperature in north-central China since 1470 AD based on drought/flood index and tree-ring records. Clim Change 110(1–2):469–498. https://doi.org/10.1007/s10584-011-0052-6

Zhang L, Zhou T (2015) Drought over East Asia: a review. J Clim 28(8):3375–3399. https://doi.org/10.1175/JCLI-D-14-00259.1

Zhao D, Zhang LX, Zhou TJ et al (2020) Contributions of local and remote atmospheric moisture fluxes to East China precipitation estimated from the CRA-40 reanalysis. J Meteor Res. doi:https://doi.org/10.1007/s13351-021-0083-5

Zong Y, Chen X (2000) The 1998 flood on the Yangtze, China. Nat Hazards 22(2):165–184. https://doi.org/10.1023/A:1008119805106